14 AC Electrochemical Sensing and Biosensing Platform Based on Biomass-Derived Macroporous Carbon Materials

DATASET · FEBRUARY 2014

9 AUTHORS, INCLUDING:

Fugang Xu
Jiangxi Normal University
58 PUBLICATIONS **1,008** CITATIONS
SEE PROFILE

Yonghai Song
Jiangxi Normal University
145 PUBLICATIONS **2,309** CITATIONS
SEE PROFILE

Shuiliang Chen
Jiangxi Normal University
53 PUBLICATIONS **911** CITATIONS
SEE PROFILE

Jianbo Jia
Chinese Academy of Sciences
72 PUBLICATIONS **2,063** CITATIONS
SEE PROFILE

analytical chemistry

Article

pubs.acs.org/ac

Electrochemical Sensing and Biosensing Platform Based on Biomass-Derived Macroporous Carbon Materials

Li Wang,[†] Qinying Zhang,[†] Shuiliang Chen,[†] Fugang Xu,[†] Shouhui Chen,[†] Jianbo Jia,[‡] Hongliang Tan,[†] Haoqing Hou,[†] and Yonghai Song*[,†]

[†]College of Chemistry and Chemical Engineering, Jiangxi Normal University, 99 Ziyang Road, Nanchang 330022, China

[‡]State Key Lab of Electroanalytical Chemistry, Changchun Institute of Applied Chemistry, Chinese Academy of Sciences, Changchun 130022, China

Supporting Information

ABSTRACT: A three-dimensional (3D) macroporous carbon (3D-KSCs) derived from kenaf stem (KS) is proposed as a novel supporting material for electrochemical sensing and a biosensing platform. A series of 3D-KSCs/inorganic nanocomposites such as Prussian blue (PB) nanoparticles (NPs)-carboxylic group-functionalized 3D-KSCs (PBNPs-3D-FKSCs), CuNiNPs-3D-KSCs, and CoNPs-3D-KSCs were prepared by a facile two-step route consisting of carbonization and subsequent chemical synthesis or one-step carbonization of KS−metal ion complex. The obtained 3D-KSCs/inorganic nanocomposites were characterized by X-ray diffraction, X-ray photoelectron spectroscopy, energy dispersive X-ray spectroscopy, scanning electron microscopy, and Fourier transform-infrared spectroscopy. A whole piece of 3D-KSCs/nanocomposites was used to prepare an integrated 3D-KSCs/nanocomposite electrode. Compared to the electrode modified by graphene, carbon nanotubes and their derivatives, which can form close-packed structure after assembled on electrode surface, the integrated 3D-KSCs/nanocomposite electrode shows a 3D honeycomb porous structure. Such structure provides a large specific surface area, effectively supports a large number of electroactive species, and greatly enhances the mass and electron transfer. The electrochemical behaviors and electrocatalytic performances of the integrated 3D-KSCs/inorganic nanocomposite electrode were evaluated by cyclic voltammetry and the amperometric method. The resulted PBNPs-3D-FKSCs, CuNiNPs-3D-KSCs, and CoNPs-3D-KSCs electrode show good electrocatalytic performances toward the reduction of H_2O_2, the oxidation of glucose and amino acid, respectively. Therefore, the low-cost, renewable, and environmentally friendly 3D-KSCs should be promising supporting materials for an electrochemical sensor and biosensor.

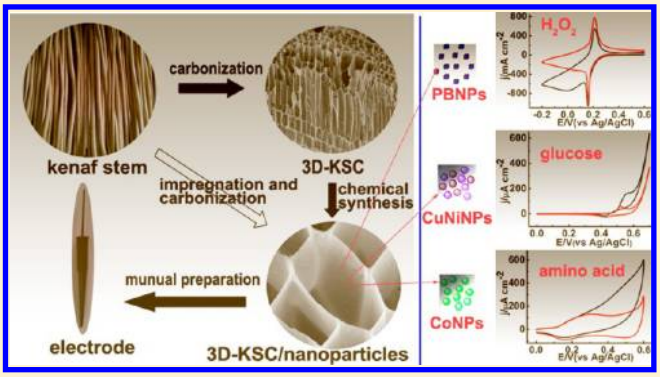

Porous carbon (PC) with a large specific surface area, accessible surface chemistry, and short diffusion pathway for mass transfer has attracted great interests due to their promising applications in electrocatalysis, energy storage, electrochemical sensor, and capacitor devices.[1−9] Zeolites, mesoporous silicas, or other porous materials with a uniform channel system are usually employed as templates to form PC[10−12] via filling precursors into the pores existing inside templates, carbonizing composites and removing the templates. PC can also be fabricated by using self-assembled molecule or supramolecule aggregates as templates via direct carbonizing templates.[13] The expensive and cockamamie preparations generally limit industrially scalable production and practical application of PC.

Recently, biomass-derived PC has attracted special attention because it can be cheaply prepared from a wide variety of low-cost precursors.[14,15] Over the past decades, lots of biomass with porous structure and miscellaneous elements have been directly carbonized to form miscellaneous elements-doped PC materials.[16,17] The porous structures are kept in the carbonization to form various PC. The doping of miscellaneous elements in PC can introduce the donor states near the Fermi level to generate n-type conductive materials, and the well-bonded miscellaneous element can drastically change the electronic performance, provide more active sites, increase the interaction between the carbon and adsorbents, and thus it is expected to improve electrochemical performance.[18] Most studies were focused on the porous features of the PC materials for potential applications in energy storage,[19,20] catalyst supports, CO_2 capture,[21] and microbial fuel cells anode.[22,23] Regretfully, the biomass-derived PC was rarely applied in electroanalytical chemistry until now.

As an important research area of analytical chemistry, electroanalytical chemistry has attracted more and more

Received: May 4, 2013
Accepted: January 15, 2014

   dx.doi.org/10.1021/ac401563m | *Anal. Chem.* XXXX, XXX, XXX−XXX

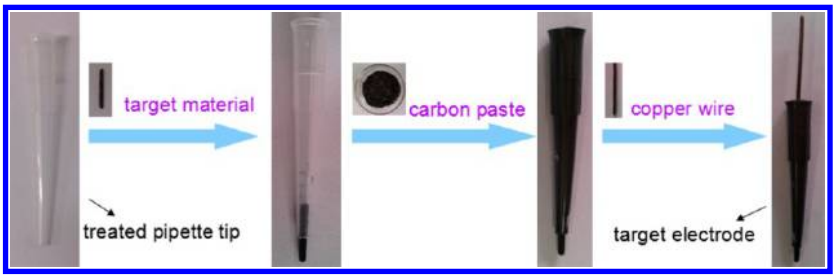

Figure 1. Schematic illustration of the fabrication of the integrated 3D-KSCs/inorganic nanocomposite electrode.

attention due to its low-cost instrumentation, high sensitivity, simplicity, rapid response, etc.[24,25] A long-term challenge of electroanalytical chemistry is effective immobilization of electro-active species on the electrode surface, which determines the detection limit, linear range, and sensitivity.[26] Over the past few decades, important advancements in electrode modification have been achieved as a result of the introduction of the graphene, carbon nanotubes (CNT), and other nanomaterials with high electronic conductivity, large specific surface area, and good catalytic activity. However, a fatal weakness is that these materials can form close-packed structures after they are assembled on an electrode surface, which will reduce their specific surface area and hinder the mass transfer.

The low-cost, renewable, and environmentally friendly three-dimensional (3D) PC (3D-KSCs) derived from kenaf stem (KS, byproducts of agricultural crops)[23] may be promising to replace carbon nanofibers (CNFs), graphene, CNT, and other nanomaterials as the supporting matrix to modify electrode for electroanalytical chemistry. To verify the proposal, a series of 3D-KSCs/inorganic nanocomposites including Prussian blue (PB) nanoparticles (NPs)-carboxylic group-functionalized 3D-KSCs (PBNPs-3D-FKSCs), CuNiNPs-3D-KSCs, and CoNPs-3D-KSCs are prepared. The common H_2O_2, glucose, cysteine, and *N*-acetyl cysteine are chosen as target molecules. A whole piece of 3D-KSCs/nanocomposites was used to prepare integrated 3D-KSCs/nanocomposite electrode. Compared to the electrode modified by graphene, CNT, and their derivatives, the integrated 3D-KSCs/nanocomposites electrode shows a 3D honeycomb porous structure. Such structure provides a large specific surface area, effectively supports a large number of electro-active species, and greatly enhances the mass and electron transfer, which improves its electroanalytical performance. The low cost, easy preparation, and good electroanalytical performance of the integrated 3D-KSCs/inorganic nanocomposite electrode indicate that the 3D-KSCs will be a kind of promising superior material for electrochemical sensing.

EXPERIMENTAL SECTION

Reagents and Materials. The KS was provided by Futian farm (Ji'an, China). $FeCl_3$, $K_3Fe(CN)_6$, KCl, HNO_3 (65%), H_2O_2 (30%), and glucose were purchased from Beijing Chemical Reagent Factory (Beijing, China). $NiCl_2{\cdot}6H_2O$, $CuCl_2$, and $Co(Ac)_2{\cdot}4H_2O$ were obtained from China National Pharmaceutical Group. *N*-Acetyl cysteine and cysteine were obtained from Sigma-Aldrich (Milwaukee, WI). All reagents (analytical grade) were used as received without further purification. Phosphate buffer solution (0.05 M) containing 0.1 M KCl (PBS, pH 6.0) was prepared with KH_2PO_4 and K_2HPO_4. Ultrapure water (18.2 MΩ cm) was purified by a Millipore-Q System.

Preparation of 3D-KSCs and FKSCs. The 3D-KSCs was obtained by carbonizing dried KS directly. The carbonization was performed in a tubular quartz reactor under N_2 atmosphere at 5 °C min^{-1} and annealed at 900 °C for 2 h. Carboxylic group-functionalized 3D-KSCs (3D-FKSCs) was prepared according to our previous method preparing carboxylic group-functionalized CNFs.[27] Briefly, a certain mass of 3D-KSCs was first heated under reflux in 15% HNO_3 at 80 °C for 3 h. Then the solid sample was removed out and rinsed by water until pH = 7.0. Finally, the product was dried at 120 °C to obtain pure 3D-FKSCs.

Preparation of PBNPs-3D-FKSCs. The PBNPs-3D-FKSCs was prepared based on previous work preparing PB-CNTs.[28] Briefly, 0.5 g of 3D-FKSCs was immersed into 10 mL of $FeCl_3$ solution. After that, 10 mL of $K_3Fe(CN)_6$ and 1.0 mL of 11.7 M HCl were successively added into the above solution, then the mixture was refluxed at 80 °C for different times. Finally, the blue stems were washed with ultrapure water and dried at 75 °C to obtain the PBNPs-3D-FKSCs.

Preparation of CuNiNPs-3D-KSCs and CoNPs-3D-KSCs. At first, 0.5 g of dried KS was immersed in 10 mL of aqueous solution containing 0.7 M $NiCl_2$ and $CuCl_2$ (c_{NiCl_2}/c_{CuCl_2} = 1:1) for about 20 days. After drying at 80 °C, the soaked KS was carbonized in a tubular quartz reactor at 900 °C for 2 h to obtain the CuNiNPs-3D-KSCs. The preparation of CoNPs-3D-KSCs was the same as CuNiNPs-3D-KSCs, except the soaking solution was replaced by 10 mL of 0.02 M $Co(Ac)_2$ and the carbonization temperature was 800 °C.

Preparation of Integrated 3D-KSCs/Inorganic Nanocomposite Electrode. The 3D-KSCs/inorganic nanocomposite electrode was prepared by the following procedure (Figure 1). First, the 3D-KSCs/inorganic nanocomposite was cut into appropriate size and put into a pretreated pipet tip. Then, 1.0 g of graphite powder and 0.25 g of liquid paraffin were mixed and well homogenized. After that, the mixture was packed firmly into the above pipet tip, and a copper wire was inserted into the pipet tip. Finally, the paste was naturally dried at room temperature before use. The resulting electrode was referred to as the 3D-KSCs/inorganic nanocomposite electrode.

Apparatus. Amperometry, electrochemical impedance spectroscopy (EIS), linear sweep voltammetry (LSV), and cyclic voltammetry (CV) were performed on a CHI660C (CH Instruments, China). A 3D-KSCs/inorganic nanocomposite electrode, a Pt wire, and an Ag/AgCl (saturated KCl) were used as the working, counter, and reference electrode, respectively. EIS was carried out in 5.0 mM $Fe(CN)_6^{3-/4-}$ containing 0.1 M KCl in the frequency of 10^5 −0.01 Hz with a amplitude of 5.0 mV under the open circuit potential. Scanning electron microscopy (SEM) analysis was performed on a XL30 ESEM-FEG SEM equipped with a Phoenix energy dispersive X-ray analyzer at an accelerating voltage of 20 kV.

dx.doi.org/10.1021/ac401563m | *Anal. Chem.* XXXX, XXX, XXX−XXX

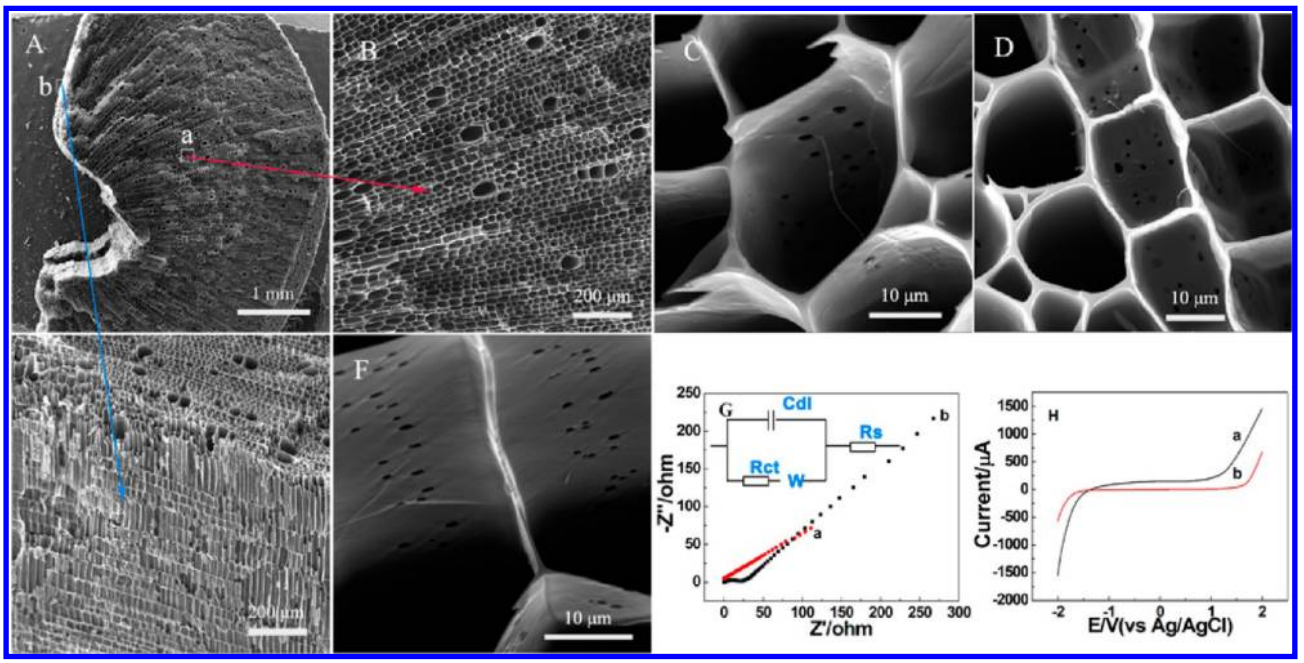

Figure 2. (A–F) SEM images of 3D-KSCs: (A) overview of a piece of cleaved 3D-KSCs, (B) top-view image, (C,D) images magnified from position B, (E) side-view image, (F) image magnified from position E, (G) Nyquist plots at the 3D-KSCs electrode (curve a) and GCE (curve b) in 5 mM $Fe(CN)_6^{3-/4-}$ containing 0.1 M KCl. The inset is the equivalent circuit. (H) LSVs of the 3D-KSCs electrode (curve a) and GCE (curve b) in 0.1 M PBS (pH 7.0) at 50 mV s^{-1}.

RESULTS AND DISCUSSION

Characterization of the 3D-KSCs. Figure 2A shows the SEM image of a piece of 3D-KSCs revealing the hollow structure inside. Highly-magnified SEM images (Figure 2B–F) indicate the well-ordered hierarchical pores. The top-view in Figure 2B reveals that two main channels are uniformly distributed in the 3D-KSCs and their diameters are about 25 and 60 μm, respectively. The side-view reveals that these channels are separated by many valves (Figure 2E). Magnified images (Figure 2C,D,F) show that these channels are throughout by a large number of pores (several micrometers) in the walls and the valves. N_2 adsorption–desorption isotherm indicates there are some micropores in the 3D-KSCs, which results in a large specific surface area (Figure S1 and Table S1, Supporting Information).

The electron transfer capability of the integrated 3D-KSCs electrode was studied by using EIS (Figure 2G). The value of electron-transfer resistance (R_{ct}) for GCE is larger than that of the 3D-KSCs electrode. The result demonstrates that the electron transfer of the 3D-KSCs electrode may be faster than that of GCE owing to the fact that its 3D honeycomb porous structure and good electric conductivity (Table S1, Supporting Information) improves the mass transfer. The available potential window of the electrode may strongly affect its further electroanalytical application,[29] and accordingly it was tested in 0.1 M pH 7.0 PBS (Figure 2H) here. As shown in Figure 2H, the working potential window of the integrated 3D-KSCs electrode is about 2.6 V, close to that of bare GCE.

Characterization of the PBNPs-3D-FKSCs. To prepare the PBNPs-3D-FKSCs, the 3D-KSCs was first oxidized into 3D-FKSCs by HNO_3 to provide carboxyl groups on its surface.[27] The morphology of 3D-FKSCs is almost intact (Figure S2, Supporting Information) after acid treatment. Figure S3A–F (Supporting Information) present the expected SEM images of the as-prepared PBNPs-3D-FKSCs. The 3D honeycomb porous structures of 3D-KSCs are kept (Figure S3A,B, Supporting Information). Moreover, the magnified images (Figure S3B–F, Supporting Information) show many PBNPs dispersed uniformly on the channel walls. The PBNPs and the functional groups result in the decrease of electric conductivity and specific surface area (Table S1, Supporting Information). The formation process is also confirmed by the photographs inserted in Figure S3A (Supporting Information) where the off-white KS was transformed into black 3D-KSCs and blue PBNPs-3D-FKSCs in sequence. The inset in Figure S3G (Supporting Information) shows that the 3D-KSCs mainly contains two elements of C and O. Energy dispersive spectroscopy (EDS) of PBNPs-3D-FKSCs reveals new elements of N and Fe, suggesting the formation of PBNPs (Figure S3G, Supporting Information). In FT-IR spectra of the 3D-KSCs (Figure S3H(a), Supporting Information), the bands around 3418, 1586, and 1237 cm^{-1} (corresponding to –OH, COO^-, and C–O, respectively) suggest some oxygen-containing groups on the 3D-KSCs. After treated by HNO_3, a new peak corresponding to C=O bonds (1738 cm^{-1}) appears in the FT-IR spectra of the 3D-FKSCs (Figure S3H(b), Supporting Information), which confirms the successful carboxylic-group functionalization of 3D-KSCs. The FT-IR spectra (Figure S3H(c), Supporting Information) of the PBNPs-3D-FKSCs presents another new peak corresponding to C≡N (2087 cm^{-1}), suggesting the successful preparation of PBNPs.

Previous reports[30−32] indicate that PBNPs can be formed directly in a $FeCl_3$–$K_3Fe(CN)_6$ mixture containing FCNFs or CNTs by spontaneously transferring electron from FCNFs or CNTs to Fe^{III}–$Fe^{III}(CN)_6^{3-}$. Similarly, in the presence of 3D-FKSCs, the electron transfer from 3D-FKSCs to the adsorbed Fe^{III}–$Fe^{III}(CN)_6^{3-}$ may also result in the formation of PBNPs. The density and size of the PBNPs in PBNPs-3D-FKSCs increase simultaneously with the increasing of $FeCl_3$–K_3Fe-

dx.doi.org/10.1021/ac401563m | Anal. Chem. XXXX, XXX, XXX–XXX

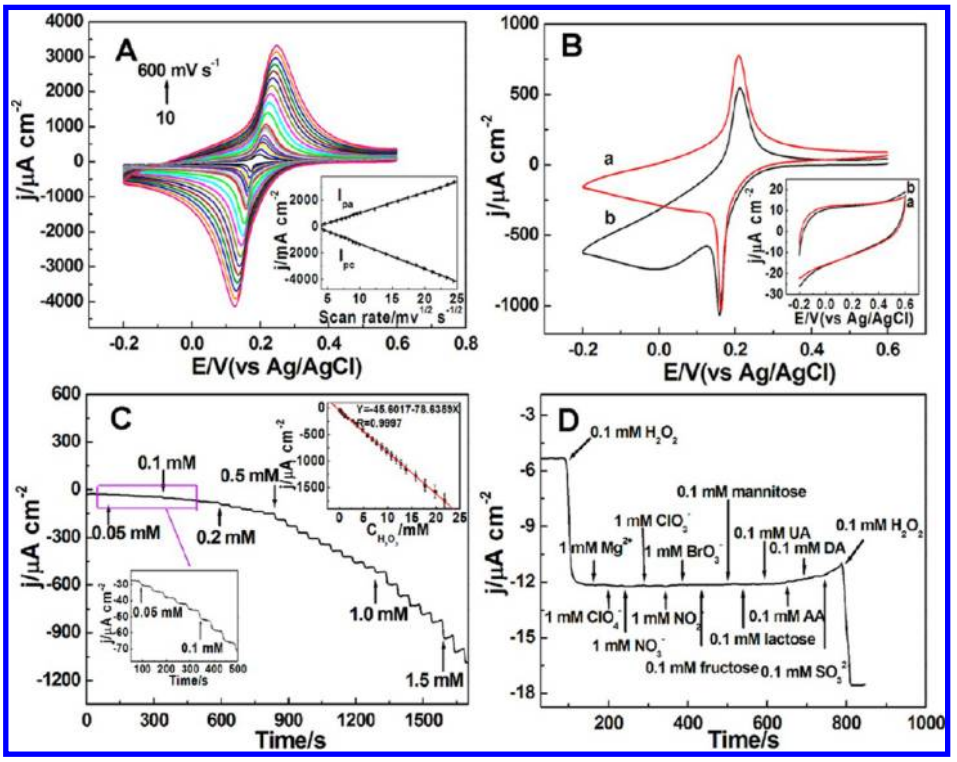

Figure 3. (A) CVs of the PBNPs-3D-FKSCs electrode in 0.05 M PBS + 0.1 M KCl (pH 6.0) at various scan rates. Inset is the plot of peak current density versus square root of scan rates. (B) CVs of the PBNPs-3D-FKSCs electrode and 3D-FKSCs electrode (inset) in the (a) absence and (b) presence of 3.0 mM H_2O_2 in 0.05 M PBS + 0.1 M KCl (pH 6.0) at 50 mV s^{-1}. (C) Amperometric response of the PBNPs-3D-FKSCs electrode upon successive addition of H_2O_2 to 0.05 M PBS + 0.1 M KCl (pH 6.0) at −0.05 V. Inset: the calibration curve. (D) Amperometric response of the PBNPs-3D-FKSCs electrode to different chemicals at −0.05 V.

$(CN)_6$ concentration (Figure S4, Supporting Information). When the concentration was 100 mM, relatively uniform steamed bun-like PBNPs were formed with an average size of about 196 nm (Figure S4C, Supporting Information). The growth process of PBNPs-3D-FKSCs over time was monitored by SEM (Figure S5, Supporting Information). At 6 h, many PBNPs were formed and some grew into nanocubes. After 12 h, most of the generated PBNPs existed in the form of cubic type, and a small number of PBNPs existed as cuboids. The crystal structure of PBNPs-3D-FKSCs nanocomposites was identified by X-ray powder diffraction (XRD) (Figure S4D, Supporting Information). The two XRD peaks at curve (a) reveal the graphitic structure of 3D-FKSCs. Peaks at 17.2°, 24.5°, 28.5°, 35.1°, 39.4°, 43.9°, 50.9°, 54.3°, and 57.4° are assigned to the (200), (220), (311), (400), (420), (422), (440), (600), and (620) facets of face centered cubic PBNPs (JCPDS No. 73-0687) (curves b−f),[33] respectively. The XPS spectra reveal the existence of N and Fe elements in the PBNPs-3D-FKSCs (Figure S6, Supporting Information). The peaks at 711.8 and 721.4 eV can be attributed to Fe^{3+} in PBNPs. The peak at 708.2 eV results from Fe^{2+} of PBNPs. The peaks at 402.4, 399.5, and 397.5 eV are assigned to N of C−N in the PBNPs-3D-FKSCs.[30] On the basis of the above results, the face centered cubic PBNPs are successfully prepared.

Characterization of the CuNiNPs-3D-KSCs and CoNPs-3D-KSCs. The CuNiNPs-3D-KSCs and CoNPs-3D-KSCs were prepared by a facile one-step carbonization of 3D-KS-metal ion complex. After the metal ion soaked 3D-KSs were carbonized under N_2 for 2 h, $NiCl_2$−$CuCl_2$/3D-KS and $Co(Ac)_2$/3D-KS were transformed into CuNiNPs-3D-KSCs and CoNPs-3D-KSCs, respectively. The SEM images (Figure S7, Supporting Information) indicate that the CuNiNPs are spherical with a main diameter of 248 nm. Some CuNiNPs embed into the 3D-KSCs, and some new holes appear which should be helpful for the electrocatalytic performances of 3D-KSCs/inorganic nanocomposites. Both the density and the size of the CuNiNPs increase simultaneously with the increasing of carbonization temperature (Figure S8, Supporting Information). EDS reveals the peaks corresponding to Ni and Cu, and the molar ratio of Ni/Cu is about 1:1 in the CuNiNPs (Figure S9, Supporting Information). The composition of the CuNiNPs-3D-KSCs was also identified by XPS spectra (Figure S10, Supporting Information). The binding energies at 932.8 and 853.6 eV are assigned to Cu^0 and Ni^0, respectively, indicating the existence of metal CuNiNPs in the CuNiNPs-3D-KSCs.[34] As well as CuNiNPs-3D-KSCs, spherical CoNPs with a main diameter of 252 nm are also distributed very well on the 3D-KSCs (Figure S11, Supporting Information). The composition of the CoNPs-3D-KSCs was also identified by XPS spectra (Figure S12, Supporting Information). The binding energies at 778.4 eV are assigned to Co^0, indicating the existence of metal CoNPs in the CoNPs-3D-KSCs.[35] In addition, XRD data also confirms the crystal structure of CuNiNPs-3D-KSCs and CoNPs-3D-KSCs (Figure S13, Supporting Information). Peaks located at 43.9°, 51.4°, and 75.2° result from (111), (200), and (220) facets of CuNi alloy (JCPDS No. 04-0850 (Ni) and 04-0836 (Cu)), respectively.[34] Peaks located at 44.1°, 51.6°, and 75.7° result from the (111), (200), and (220) facets of Co (JCPDS No. 01-1255),[35] and peaks located at 36.3° can be indexed to the (111) facets of Co_3O_4 (JCPDS No. 43-1003).[35] The results demonstrate the successful synthesis of the

dx.doi.org/10.1021/ac401563m | Anal. Chem. XXXX, XXX, XXX−XXX

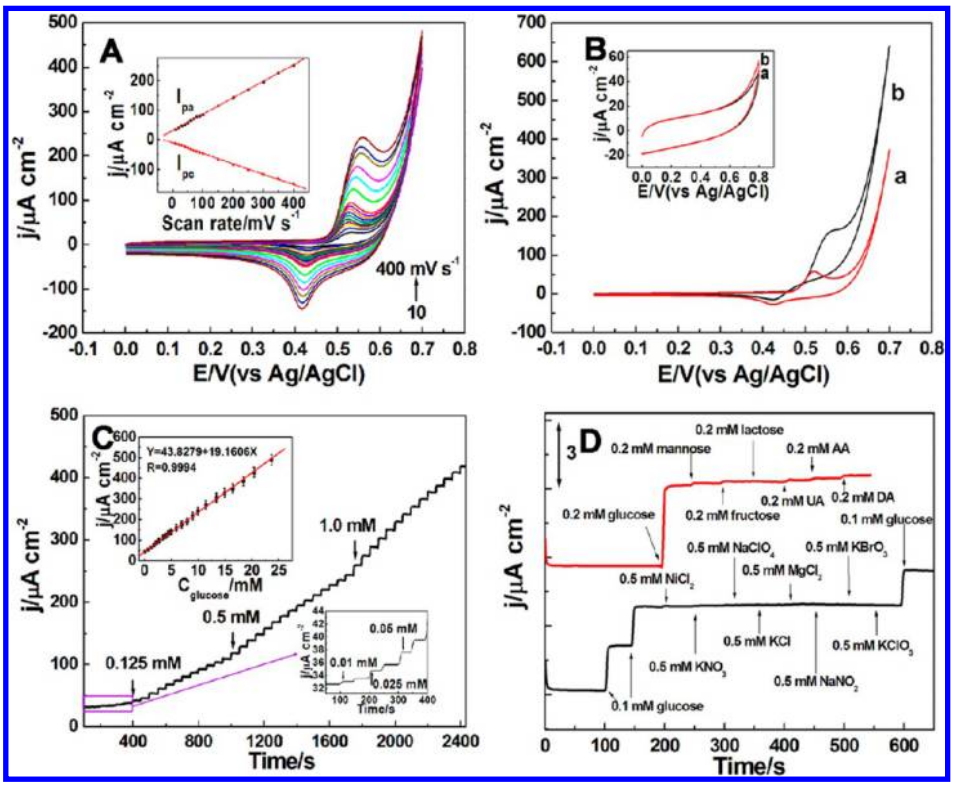

Figure 4. (A) CVs of the CuNiNPs-3D-KSCs electrode in 0.1 M NaOH at various scan rates. Inset is the plot of peak current density versus scan rates. (B) CVs of the CuNiNPs-3D-KSCs electrode and 3D-KSCs electrode (Inset) in the (a) absence and (b) presence of 2.0 mM glucose in 0.1 M NaOH at 50 mV s^{-1}. (C) Amperometric response of the CuNiNPs-3D-KSCs electrode upon successive addition of glucose to 0.1 M NaOH at 0.55 V. Inset: the calibration curve. (D) Amperometric response of the CuNiNPs-3D-KSCs electrode to different chemicals in a stirring 0.1 M NaOH at 0.55 V.

3D-KSCs/inorganic nanocomposites by a facile one-step carbonization of 3D-KS−metal ion complex.

Electrochemical Behaviors and Electrocatalytics of the Integrated PBNPs-3D-FKSCs Electrode toward H_2O_2. In many biological and environmental processes, H_2O_2 is an important intermediate species.[36,37] Therefore, the accurate determination of H_2O_2 is of practical importance. Since the PBNPs is usually considered as an artificial peroxide enzyme, the PBNPs-3D-FKSCs is used to construct H_2O_2 sensor and to test if the 3D-KSCs can be used as supporting matrix for preparing electrochemical sensors. Figure 3A shows the CVs of the integrated PBNPs-3D-FKSCs electrode in 0.05 M PBS + 0.1 M KCl (pH 6.0) at a scan rate ranging from 10 to 600 mV s^{-1}. The peak current density increased linearly with the square root of scan rate (inset in Figure 3A), suggesting a diffusion-controlled process. According to previous results,[30] after the as-prepared $Fe^{III}_4[Fe^{II}(CN)_6]_3$ (PB) was potentially scanned in 0.05 M PBS + 0.1 M KCl (pH 6.0), the $Fe^{III}_4[Fe^{II}(CN)_6]_3$ was transformed into $KFe^{III}[Fe^{II}(CN)_6]$ (new PB) by replacing Fe^{3+} with K^+. The redox process of PBNPs-3D-FKSCs nanocomposites was accompanied by the dissolution and association of K^+. Therefore, the slow transfer of K^+ resulted in the diffusion-controlled electrochemical process. The redox peak in Figure 3A might result from the transformation of new PBNPs and Prussian white (PW; $K_2Fe^{II}[Fe^{II}(CN)_6]$[30]). Figure 3B shows the CVs of the PBNPs-3D-FKSCs electrode in 0.05 M PBS + 0.1 M KCl (pH 6.0) without (curve a) and with (curve b) 3.0 mM H_2O_2. It clearly showed that the current density of the reduction peak at about −0.05 V increased greatly after 3.0 mM H_2O_2 was added. The enhancement was superior to that of the 3D-FKSCs electrode (inset in Figure 3B). Obviously, the reduction of H_2O_2 was catalyzed by PWNPs[30] with a mechanism as follows:[38,39]

$$KFe^{III}[Fe^{II}(CN)_6] + K^+ + e^- \rightarrow K_2Fe^{II}[Fe^{II}(CN)_6] \quad (1)$$

$$2K_2Fe^{II}[Fe^{II}(CN)_6] + H_2O_2 + 2H^+ \rightarrow 2KFe^{III}[Fe^{II}(CN)_6] + 2H_2O + 2K^+ \quad (2)$$

In this mechanism, PBNPs was first reduced to PWNPs on the electrode and then the PWNPs reduced H_2O_2 into H_2O in a solution with the regeneration of PBNPs. The integrated PBNPs-3D-FKSCs electrode effectively supports a large number of PBNPs, and the honeycomb porous structure is beneficial for mass transfer. The synergetic effect between 3D-FKSCs and PBNPs might improve the catalytic activity of PBNPs. Thus, the 3D-KSCs would be a good supporting matrix to prepare electrochemical sensors. Some experimental conditions were optimized to obtain the best sensitivity in Figure S14 (Supporting Information). Figure 3C shows the amperometric response of the PBNPs-3D-FKSCs electrode toward H_2O_2 under the optimal conditions. The current response was enhanced as a small quantity of H_2O_2 was added. The current density was proportional to H_2O_2 concentration in 1.0 μM −21.75 mM (r = 0.9997). The detection sensitivity was 78.64 μA cm^{-2} mM^{-1}, and the detection limit was 0.1 μM (S/N = 3) (inset in Figure 3C). Compared to some previous sensors based on PB modified electrode, the integrated PBNPs-3D-FKSCs electrode shows the best linear range (Table S2, Supporting Information). The medium sensitivity may be ascribed to the fact that the sensitivity not only depends on the

dx.doi.org/10.1021/ac401563m | Anal. Chem. XXXX, XXX, XXX−XXX

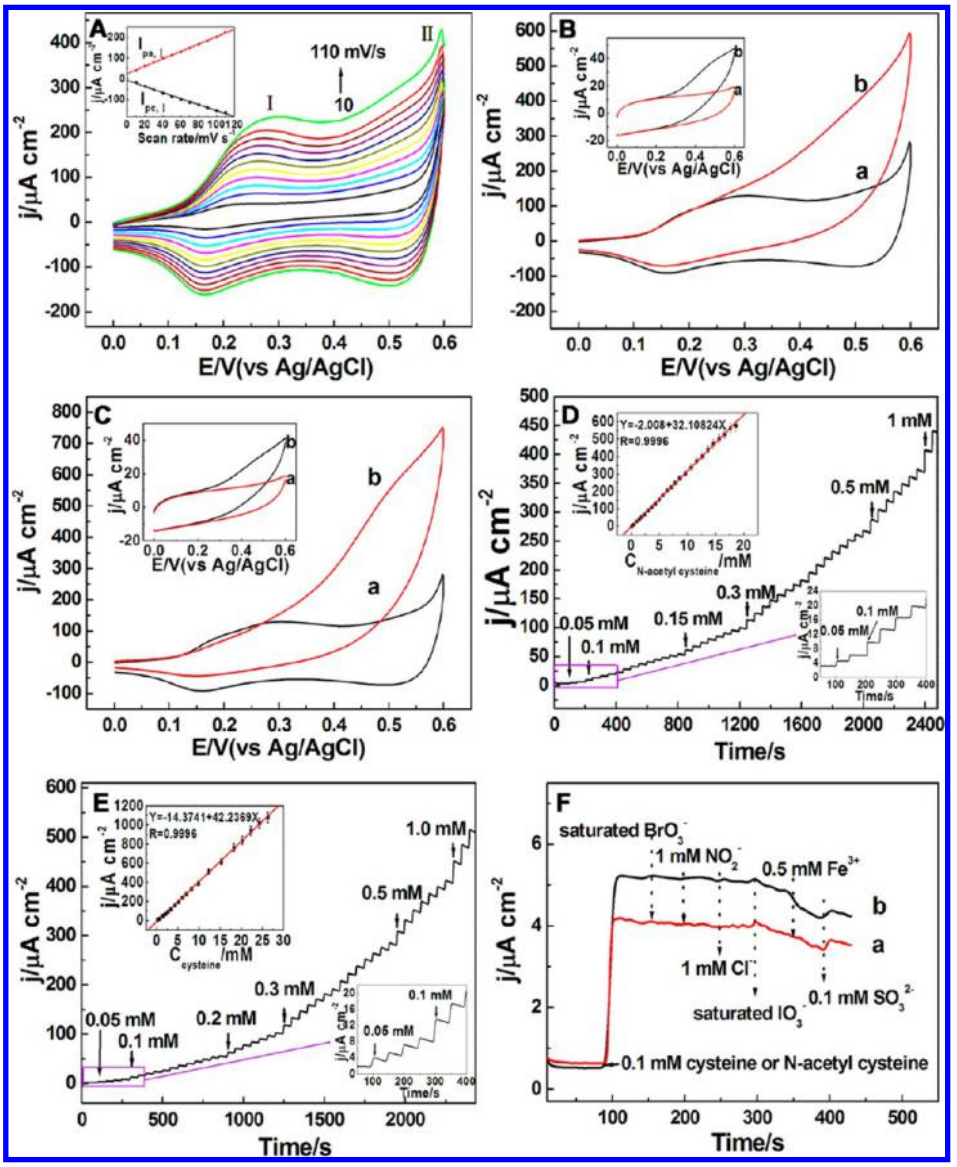

Figure 5. (A) CVs of the CoNPs-3D-KSCs electrode in 0.1 M NaOH at various scan rates. The inset is the plot of peak current density versus scan rates. (B,C) CVs of the CoNPs-3D-KSCs electrode and 3D-KSCs electrode (inset) in the (a) absence and (b) presence of 3.0 mM *N*-acetyl cysteine (B) and cysteine (C) in 0.1 M NaOH at 50 mV s^{-1}. (D,E) Amperometric response of the CoNPs-3D-KSCs electrode upon successive addition of (D) *N*-acetyl cysteine and (E) cysteine to 0.1 M NaOH at 0.55 V. Inset: the calibration curve. (F) Amperometric response of the CoNPs-3D-KSCs electrode to different chemicals: (a) *N*-acetyl cysteine, BrO_3^-, NO_2^-, Cl^-, IO_3^-, Fe^{3+}, SO_3^{2-} and (b) cysteine, BrO_3^-, NO_2^-, Cl^-, IO_3^-, Fe^{3+}, SO_3^{2-} in stirring 0.1 M NaOH at 0.55 V.

electrode construction but also depends on the properties of electro-active species.

As shown in Figure 3D, some possibly coexisted chemicals did not show interference to H_2O_2 detection. The stability of the sensor was estimated by detecting 1.0 mM H_2O_2 after it was stored at 4 °C for 50 days, and the current density only decreased by 2.1%. H_2O_2 (1.0 mM) was successively checked for 5 times at one electrode and yielded a relative standard deviation (RSD) value of 3.3%. The 1.0 mM H_2O was determined at five different electrodes to estimate the electrode-to-electrode reproducibility and gave a RSD of 6.4%. The results suggest that the integrated PBNPs-3D-FKSCs electrode is stable and repeatable and can selectively detect H_2O_2.

Electrochemical Behaviors and Electrocatalytics of the Integrated CuNiNPs-3D-KSCs Electrode toward Glucose. Figure 4A shows the CVs of the integrated CuNiNPs-3D-KSCs electrode in 0.1 M NaOH at scan rate ranging from 10 to 400 mV s^{-1}. The peak current density increased proportionally as the scan rate increased (inset in Figure 4A), suggesting a surface-controlled process. The electron-transfer number (n) and electron-transfer coefficient (α_s) were obtained according to Laviron's theory:[40]

$$E_{pc} = E^{0'} + \frac{RT}{\alpha_s nF} - \frac{RT}{\alpha_s nF} \ln \upsilon \quad (3)$$

$$E_{pa} = E^{0'} + \frac{RT}{(1-\alpha_s)nF} + \frac{RT}{(1-\alpha_s)nF} \ln \upsilon \quad (4)$$

where R is the gas constant (R = 8.314 J mol^{-1} K^{-1}), n is the electron transfer number, F is the Faraday constant (F = 96 493 C mol^{-1}), and T is the temperature in Kelvin (T = 298 K).

dx.doi.org/10.1021/ac401563m | *Anal. Chem.* XXXX, XXX, XXX–XXX

According to the plots of cathodic peak potential (E_{pc}) and anodic peak potential (E_{pa}) versus the natural logarithm of the scan rate (ln υ) (Figure S15, Supporting Information), the $\alpha_s n$ was calculated to be 0.687. The α_s should be $0.3 < \alpha < 0.7$, thus the α_s and n was calculated to be 0.687 and 1, respectively, suggesting a single electron transfer process. On the basis of these results and previous conclusion,[41] the electrochemical reactions were expressed as[41]

$$Cu(OH)_2 + OH^- \rightarrow CuOOH + H_2O + e \quad (5)$$

$$Ni(OH)_2 + OH^- \rightarrow NiOOH + H_2O + e \quad (6)$$

In 0.1 M NaOH solution, the CuNiNPs can easily transform into $Cu(OH)_2$ and $Ni(OH)_2$. Then under high potential, the $Cu(OH)_2$ and $Ni(OH)_2$ can be further oxidized to generate a large number of CuOOH and NiOOH, which can oxidize glucose to gluconolactone. Figure 4B shows the CVs of the CuNiNPs-3D-KSCs electrode in 0.1 M NaOH in the absence (curve a) and presence (curve b) of 2.0 mM glucose at 50 mV s^{-1}. The oxidation peak at 0.55 V increased greatly, and the reduction peak at 0.43 V decreased slightly after the addition of 2.0 mM glucose, while the oxidation peak was much smaller at the 3D-KSCs electrode (inset in Figure 4B). The results indicate that the current density mainly results from the oxidation of glucose catalyzed by active CuOOH and NiOOH. Some experimental conditions were optimized (Figure S16, Supporting Information). Figure 4C shows the amperometric response of the CuNiNPs-3D-KSCs electrode for successive addition of glucose under the optimal conditions. On the basis of the experimental result, a linear range of 7.0 μM to 23.67 mM (r = 0.9994), a sensitivity of 19.16 μA cm^{-2} mM^{-1} and a detection limit of 2.3 μM (S/N = 3) (inset) were obtained. Our newly designed sensor was much better than those previously developed ones for glucose assay (Table S3, Supporting Information).

The interference from some possible chemicals in human serum samples was tested. As shown in Figure 4D, some usual inorganic ions did not interfere with glucose detection. The addition of lactose provided slight interference for glucose sensing, and mannose, fructose, uric acid (UA), ascorbic acid (AA), and dopamine (DA) made a poor increase of currents (<10%), indicating that the proposed electrode could be used to detect glucose selectively. The detection of glucose in blood serum samples indicated the sensor performed very well (Table S4, Supporting Information). The stability of the sensor was estimated by testing 1.0 mM glucose after it was stored at 4 °C for 60 days, and the current density only decreased by 3.4%. The results suggest that the integrated CuNiNPs-3D-KSCs electrode is stable and can be used to selectively detect glucose in a practical sample.

Electrochemical Behaviors and Electrocatalytics of the CoNPs-3D-KSCs Electrode toward Amino Acids. Figure 5A shows the CVs of the integrated CoNPs-3D-KSCs electrode in 0.1 M NaOH at a scan rate ranging from 10 to 110 mV s^{-1}, suggesting it is also a surface-controlled process (inset in Figure 5A). According to previous results and n determined based on Laviron's theory (Figure S17, Supporting Information), the two redox peaks involved with the following electrochemical reaction:[42]

$$\text{Peak I:} \quad 3Co(OH)_2 + 2OH^- \rightarrow Co_3O_4 + 4H_2O + 2e \quad (7)$$

$$\text{Peak II:} \quad Co_3O_4 + H_2O + OH^- \rightarrow 3CoOOH + e \quad (8)$$

$$CoOOH + OH^- \rightarrow CoO_2 + H_2O + e \quad (9)$$

The CoO_2 can be used as catalyst for the electrocatalytic oxidation of an amino acid. Figure 5B,C shows the CVs of the CoNPs-3D-KSCs electrode in 0.1 M NaOH without (curve a) and with (curve b) 3.0 mM of *N*-acetyl cysteine (Figure 5B) and cysteine (Figure 5C), respectively, revealing a good electrocatalytic performance. Some experimental conditions were optimized in Figure S18 (Supporting Information). Under the optimal conditions, amperometric tests were carried at 0.55 V at the CoNPs-3D-KSCs electrode by the addition of *N*-acetyl cysteine (Figure 5D) or cysteine (Figure 5E) into a stirred 0.1 M NaOH, respectively. On the basis of the calibration curve obtained from the above amperometric results (inset in Figure 5D,E), the linear range of the *N*-acetyl cysteine sensor was from 0.10 to 18.60 mM (r = 0.9996) with a sensitivity of 32.11 μA cm^{-2} mM^{-1} and a detection limit of 0.05 mM. The linear range of cysteine sensor was from 0.15 to 26.24 mM (r = 0.9996) with a sensitivity of 42.24 μA cm^{-2} mM^{-1} and a detection limit of 0.02 mM. The results also were much better than some other reported ones (Table S5, Supporting Information). Figure 5F showed that chemicals such as BrO_3^-, Cl^-, NO_2^-, and IO_3^- in a 10-fold concentration did not obviously interfere with the two analytes detection. The repeatability of one sensor to five tests of 1.0 mM *N*-acetyl cysteine and cysteine yield a RSD of 2.2% and 2.3%, respectively, confirming that the sensor was stable. The reproducibility of CoNPs-3D-KSCs electrodes at 1.0 mM *N*-acetyl cysteine and cysteine was determined by testing five different sensors and gave a RSD of 2.1% and 2.3%, respectively. After the sensor was stored in a inverted beaker at 4 °C for 60 days, the current response to 1.0 mM *N*-acetyl cysteine and cysteine only decreased 3.1% and 3.5%, respectively, further suggesting the sensor's good stability.

CONCLUSIONS

In summary, a facile and industrially scalable approach to prepare honeycomb 3D-KSCs by the pyrolysis of biomass KS was proposed. The prepared 3D-KSCs can be used as a suitable supporting material for electrochemical sensing and a biosensing platform. By decorating it with various inorganic nanomaterials, the integrated 3D-KSCs/inorganic nanocomposites electrode with 3D honeycomb structure exhibits good electrocatalytic activity toward corresponding target molecules, which can be used to fabricate advanced electrochemical sensors with high sensitivity, good selectivity, and stability. Moreover, the preparation of 3D-KSCs and its composites are low cost, environmentally friendly, and available in large quantity. Thus the 3D-KSCs might be used as an advanced electrochemical sensing platform to fabricate various sensors, promising for the routine sensing and biosensing application.

ASSOCIATED CONTENT

Supporting Information

Additional information as noted in text. This material is available free of charge via the Internet at http://pubs.acs.org.

AUTHOR INFORMATION

Corresponding Author

*Phone/fax: +86-791-88120862. E-mail: yhsong@jxnu.edu.cn.

Notes

The authors declare no competing financial interest.

dx.doi.org/10.1021/ac401563m | *Anal. Chem.* XXXX, XXX, XXX−XXX

■ ACKNOWLEDGMENTS

This work was financially supported by National Natural Science Foundation of China (Grant 20905032, 21065005, and 21165010), Young Scientist Foundation of Jiangxi Province (Grants 20112BCB23006 and 20122BCB23011), the State Key Laboratory of Electroanalytical Chemistry (Grant SKLEAC201310) and Foundation of Jiangxi Educational Committee (Grants GJJ13243 and GJJ13244).

■ REFERENCES

(1) Ding, L. X.; Wang, A. L.; Li, G. R.; Liu, Z. Q.; Zhao, W. X.; Su, C. Y.; Tong, Y. X. *J. Am. Chem. Soc.* **2012**, *134*, 5730−5733.
(2) Bai, J.; Lu, B. P.; Bo, X. J.; Guo, L. P. *Electrochem. Commun.* **2010**, *12*, 1563−1567.
(3) Ndamanisha, J. C.; Guo, L. P. *Bioelectrochemistry* **2009**, *77*, 60−63.
(4) Wang, H.; Bo, X. J.; Bai, J.; Wang, L. X.; Guo, L. P. *J. Electroanal. Chem.* **2011**, *662*, 281−287.
(5) Zhang, F.; Li, G. D.; Chen, J. S. *J. Colloid Interface Sci.* **2008**, *327*, 108−114.
(6) Gao, S. Y.; Jia, X. X.; Yang, J. M.; Wei, X. *J. Mater. Chem.* **2012**, *22*, 21733−21739.
(7) Zhang, X. J.; Gu, A. X.; Wang, G. F.; Huang, Y. H.; Ji, H. Q.; Fang, B. *Analyst* **2011**, *136*, 5175−5180.
(8) Ma, T. Y.; Liu, L.; Yuan, Z. Y. *Chem. Soc. Rev.* **2012**, *42*, 3977−4003.
(9) Qin, Y.; Zhang, F.; Chen, Y.; Zhou, Y. J.; Li, J.; Zhu, A. W.; Luo, Y. P.; Tian, Y.; Yang, J. H. *J. Phys. Chem.* **2012**, *116*, 11994−12000.
(10) Han, Y. J.; Stucky, G. D.; Butler, A. *J. Am. Chem. Soc.* **1999**, *121*, 9897−9898.
(11) Teng, Z. G.; Zheng, G. F.; Dou, Y. Q.; Li, W.; Mou, C. Y.; Zhang, X. H.; Asiri, A. M.; Zhao, D. Y. *Angew. Chem., Int. Ed.* **2012**, *51*, 2173−2177.
(12) Asefa, T. *Angew. Chem., Int. Ed.* **2012**, *51*, 2008−2010.
(13) Zhang, F. Q.; Gu, D.; Yu, T.; Zhang, F.; Xie, S. H.; Zhang, L. J.; Deng, Y. H.; Wan, Y.; Tu, B.; Zhao, D. Y. *J. Am. Chem. Soc.* **2007**, *129*, 7746−7747.
(14) White, R. J.; Budarin, V.; Luque, R.; Clark, J. H.; Macquarrie, D. J. *Chem. Soc. Rev.* **2009**, *38*, 3401−3418.
(15) Sevilla, M.; Fuertes, A. B.; Mokaya, R. *Energy Environ. Sci.* **2011**, *4*, 1400−1410.
(16) Kurosaki, F.; Koyanaka, H.; Tsujimoto, M.; Imamura, Y. *Carbon* **2008**, *46*, 850−857.
(17) Li, J.; Xu, Q.; Wang, J.; Jiao, J.; Zhang, Z. *Ind. Eng. Chem. Res.* **2008**, *47*, 7680−7685.
(18) Stein, A.; Wang, Z.; Fierke, M. A. *Adv. Mater.* **2009**, *21*, 265−293.
(19) Sevilla, M.; Fuertes, A. B.; Mokaya, R. *Energy Environ. Sci.* **2011**, *4*, 1400−1410.
(20) Balatnanigaimani, M. S.; Shim, W. G.; Kim, T. H.; Cho, S. J.; Lee, J. W.; Moon, H. *Catal. Today* **2009**, *146*, 234−240.
(21) Sevilla, M.; Fuertes, A. B. *Energy Environ. Sci.* **2011**, *41*, 1765−1771.
(22) Chen, S.; Liu, Q.; He, G. H.; Zhou, Y.; Hanif, M.; Peng, X.; Wang, S. Q.; Hou, H. Q. *J. Mater. Chem.* **2012**, *22*, 18609−18613.
(23) Chen, S. L.; He, G. H.; Hu, X. W.; Xie, M. Y.; Wang, S. Q.; Zeng, D. J.; Hou, H. Q.; Schroder, U. *ChemSusChem.* **2012**, *5*, 1059−1063.
(24) Wang, J. *Chem. Rev.* **2008**, *108*, 814−825.
(25) Dai, Z.; Liu, H.; Shen, Y. D.; Su, X. P.; Xu, Z. L.; Sun, Y. M.; Zou, X. Y. *Anal. Chem.* **2012**, *84*, 8157−8163.
(26) Huang, J.; Zhang, L.; Liang, R. P.; Qiu, J. D. *Biosens. Bioelectron.* **2013**, *41*, 430−435.
(27) Cui, K.; Song, Y. H.; Guo, Q. H.; Xu, F. G.; Zhang, Y.; Shi, Y.; Wang, L.; Hou, H. Q.; Li, Z. *Sens. Actuators, B* **2011**, *160*, 435−440.
(28) Wang, T.; Fu, Y. C.; Bu, L. J.; Qin, C.; Meng, Y.; Chen, C.; Ma, M.; Xie, Q. J.; Yao, S. Z. *J. Phys. Chem.* **2012**, *116*, 20908−20917.
(29) Kato, D.; Sekioka, N.; Ueda, A.; Kurita, R.; Hirono, S.; Suzuki, K.; Niwa, O. *J. Am. Chem. Soc.* **2008**, *130*, 3716−3717.
(30) Wang, L.; Ye, Y. J.; Zhu, H. Z.; Song, Y. H.; He, S. J.; Xu, F. G.; Hou, H. Q. *Nanotechnology* **2012**, *23*, 455502.
(31) Zhang, W.; Wang, L. L.; Zhang, N.; Wang, G. F.; Fang, B. *Electroanalysis* **2009**, *21*, 2325−2330.
(32) Zhai, J. F.; Zhai, Y. M.; Wen, D.; Dong, S. *Electroanalysis* **2009**, *21*, 2207−2212.
(33) Cao, L. Y.; Liu, Y. L.; Zhang, B. H.; Lu, L. H. *ACS Appl. Mater. Interfaces* **2010**, *2*, 2339−2346.
(34) Chen, S.; Brown, L.; Levendorf, M.; Cai, W.; Ju, S.-Y.; Edgeworth, J.; Li, X.; Magnuson, C. W.; Velamakanni, A.; Piner, R. D.; Kang, J.; Park, J.; Ruoff, R. S. *ACS Nano* **2011**, *2*, 1321−1327.
(35) Noh, H.-B.; Lee, K.-S.; Chandra, P.; Won, M.-S.; Shim, Y.-B. *Electrochim. Acta* **2012**, *61*, 36−43.
(36) Luo, Y. L.; Lu, W. B.; Chang, G. H.; Liao, F.; Sun, X. P. *Electrochim. Acta* **2011**, *56*, 8371−8374.
(37) Li, J.; Qiu, J. D.; Xu, J. J.; Chen, H. Y.; Xia, X. H. *Adv. Funct. Mater.* **2007**, *17*, 1574−1580.
(38) Haghighi, B.; Hamidi, H.; Gorton, L. *Sens. Actuators, B* **2010**, *147*, 270−276.
(39) Zhang, Y.; Sun, X. M.; Zhu, L. Z.; Shen, H. B.; Jia, N. Q. *Electrochim. Acta* **2011**, *56*, 1239−1245.
(40) Laviron, E. *J. Electroanal. Chem.* **1979**, *101*, 19−28.
(41) Toghill, K. E.; Compton, R. G. *Int. J. Electrochem. Sci.* **2010**, *5*, 1246−1301.
(42) Tabeshnia, M.; Rashvandavei, M.; Amini, R.; Pashaee, F. *J. Electroanal. Chem.* **2010**, *647*, 181−186.